Chemistry–A European Journal

Research Article
doi.org/10.1002/chem.202301708

Chemistry Europe
European Chemical
Societies Publishing

www.chemeurj.org

Special Collection

Nanocomposite Hydrogels with Self-Assembling Peptide-Functionalized Carbon Nanostructures

Petr Rozhin,[a] Simone Adorinni,[a] Daniel Iglesias,[a] Tino Mackiol,[a] Slavko Kralj,[b, c] Matteo Bisetto,[a, d] Michela Abrami,[e] Mario Grassi,[e] Manuela Bevilacqua,[f, g] Paolo Fornasiero,[a, d] and Silvia Marchesan*[a, d]

To Professor Maurizio Prato for his 70th birthday

Carbon nanostructures (CNSs) are attractive components to attain nanocomposites, yet their hydrophobic nature and strong tendency to aggregate often limit their use in aqueous conditions and negatively impact their properties. In this work, carbon nanohorns (CNHs), multi-walled carbon nanotubes (CNTs), and graphene (G) are first oxidized, and then reacted to covalently anchor the self-assembling tripeptide L-Leu-D-Phe-D-Phe to improve their dispersi-

bility in phosphate buffer, and favor the formation of hydrogels formed by the self-organizing L-Leu-D-Phe-D-Phe present in solution. The obtained nanocomposites are then characterized by transmission electron microscopy (TEM), oscillatory rheology, and conductivity measurements to gain useful insights as to the key factors that determine self-healing ability for the future design of this type of nanocomposites.

[a] P. Rozhin, S. Adorinni, Dr. D. Iglesias, T. Mackiol, M. Bisetto, Prof. P. Fornasiero, Prof. S. Marchesan
Department of Chemical and Pharmaceutical Sciences
University of Trieste
Via L. Giorgieri 1, 34127 Trieste (Italy)
E-mail: smarchesan@units.it

[b] Dr. S. Kralj
Department of Materials Synthesis
Jožef Stefan Institute
Jamova 39, 1000 Ljubljana (Slovenia)

[c] Dr. S. Kralj
Department of Pharmaceutical Technology, Faculty of Pharmacy
University of Ljubljana
Aškerčeva 7, 1000 Ljubljana (Slovenia)

[d] M. Bisetto, Prof. P. Fornasiero, Prof. S. Marchesan
National Interuniversity Consortium of Materials Science and Technology (INSTM)
Unit of Trieste
Via L. Giorgieri 1, 34127 Trieste (Italy)

[e] Dr. M. Abrami, Prof. M. Grassi
Department of Engineering and Architecture
University of Trieste
Via Valerio 6/A, 34127 Trieste (Italy)

[f] Dr. M. Bevilacqua
Institute for the Chemistry of Organometallic Compounds (ICCOM-CNR)
National Research Council (CNR)
Via Madonna del Piano 10, 50019 Sesto Fiorentino (FI) (Italy)

[g] Dr. M. Bevilacqua
Third Parties Research Unit (URT-ICCOM), Department of Chemical and Pharmaceutical Sciences
University of Trieste
Via L. Giorgieri 1, 34127 Trieste (Italy)

Introduction

Over the last four decades, carbon nanostructures (CNSs) have attracted researchers' interest for their peculiar physico-chemical properties.[1] CNSs are highly heterogeneous, and they include quasi-spherical particles such as fullerenes[2] and nano-onions,[3] mono-dimensional carbon nanotubes (CNTs),[4] two-dimensional graphene (G) and derivatives,[5] and many other types of structures, such as carbon dots[6] and nanohorns.[7] In general, carbon allotropes that are sp²-hybridized display similar features, including electric conductivity and high resilience, as well as a high surface area and low density. Furthermore, they are amenable to various types of chemical functionalization for the fine-tuning of their properties, as needed depending on the specific type of envisaged use.[8] However, each CNS displays a particular morphology, size, curvature, and, thus, reactivity towards chemical derivatization. Regardless of numerous research endeavours in the area for their tailored use, often it is not possible to anticipate which CNS will provide the optimal performance, with dissimilarities being found among allotropes.[9]

Amongst CNSs' attractive properties, their conductivity bears high potential to improve (bio) materials features[10] to engineer human conductive tissues,[11] including the difficult nerve[12] and heart[13] tissues, and also to develop sensors,[14] novel catalysts,[15] and sustainable solutions in the field of energy.[16] For applications in medicine, the combination of CNSs with peptides is raising more and more attention, since it enables to combine the excellent mechanical and physical properties of the former, with the biocompatibility and bioactivity of the latter.[17] In particular, addition of self-assembling peptides to CNSs is gaining momentum, thanks to the possibility to attain multiple functionalities, and also new properties and responsive behavior towards smart and hybrid materials.[18]

Chem. Eur. J. **2023**, *29*, e202301708 (1 of 7)

© 2023 The Authors. Chemistry - A European Journal published by Wiley-VCH GmbH

Chemistry–A European Journal

Research Article
doi.org/10.1002/chem.202301708

Chemistry Europe
European Chemical
Societies Publishing
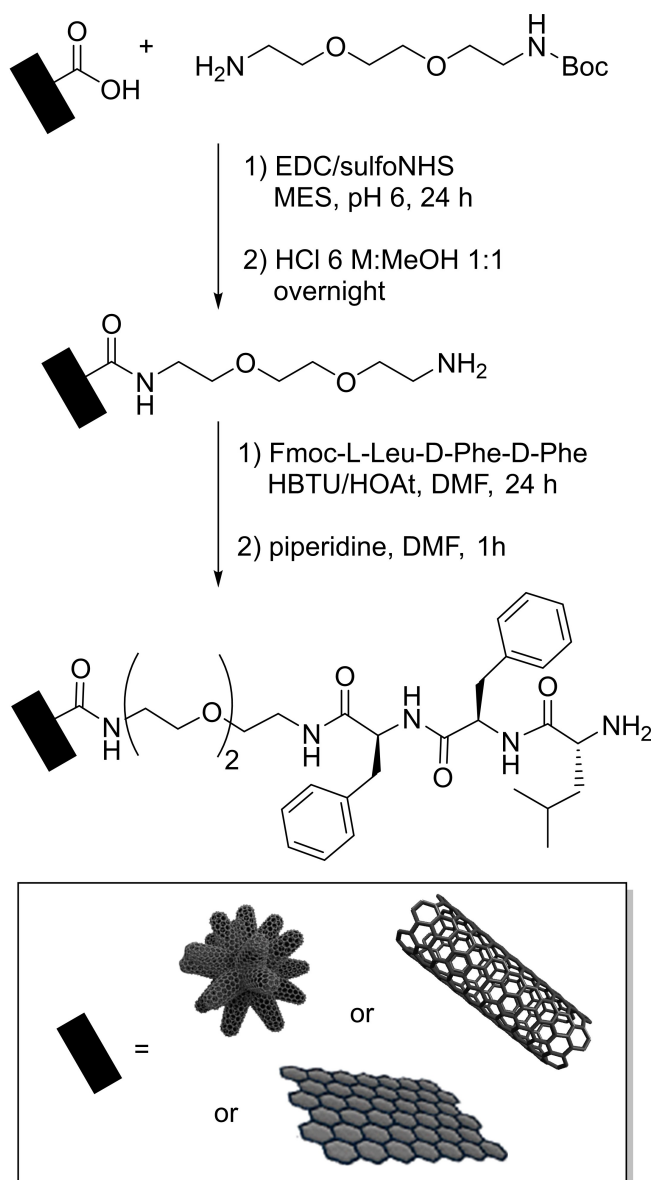
Scheme 1. Covalent functionalization strategy to attach the tripeptide gelator L-Leu-D-Phe-D-Phe to the CNSs shown in the inset (*i.e.*, MWCNTs, CNHs, GO).

A popular class of minimalistic self-assembling peptides exploits phenylalanine (Phe),[19] and provided effective gelators.[20] In this regard, the heterochiral tripeptide L-Leu-D-Phe-D-Phe was reported to self-assemble into supramolecular hydrogels at physiological conditions, and it was combined with a series of oxidized CNSs to attain nanocomposite hydrogels.[21] Interestingly, in the case of oxidized multiwalled CNTs (oxCNTs) and graphene oxide (GO), the resulting nanocomposites were highly homogeneous and with significantly improved viscoelastic properties. In addition, only the hydrogel with oxCNTs displayed self-healing ability. By contrast, in the case of oxidized carbon nanohorns (oxCNHs), the CNSs displayed a strong tendency towards self-aggregation that negatively affected the properties of the soft matter. Furthermore, it was found that, prior to triggering self-assembly, the peptide fully coated oxCNTs and GO flakes, but only partially coated the surface of the oxCNHs. It was inferred that both CNSs' morphology and the ability of the peptide to coat their surface were key factors in determining the nanocomposite homogeneity and properties. However, it was unclear as to which factors were required to attain the self-healing ability. To shed light on these aspects, in this work, we explored the covalent attachment of L-Leu-D-Phe-D-Phe onto the different CNSs to favor their interaction with the free peptide and reduce CNS aggregation, providing an alternative strategy towards nanocomposites, and to gain a deeper understanding of these systems at the interface between nanotechnology and supramolecular chemistry.

Results and Discussion

CNS covalent functionalization

The tripeptide Fmoc- L-Leu-D-Phe-D-Phe was prepared according to a typical procedure in solid phase, followed by purification by trituration.[22] To covalently attach Fmoc- L-Leu-D-Phe-D-Phe onto the CNSs, the short linker 2,2′-(ethylenedioxy)bis(ethylamine) was employed as shown in Scheme 1. Briefly, each CNS was first oxidized to the same level of oxygen content as confirmed by thermogravimetric analysis (TGA), with a weight loss of ~10% at 600°C, using previously optimized protocols in acidic solutions.[21] Next, the introduced COOH functionalities (*i.e.*, 2.5 ± 0.2 mmol COOH/g assuming these were the predominant functional groups on the nanocarbons' surface)[21] were reacted with the N-Boc monoprotected linker through amidation. Subsequent N-Boc deprotection released a free primary amine group that could be used to couple the N-capped Fmoc-L-Leu-D-Phe-D-Phe from the C-terminus, so that subsequent Fmoc-deprotection yielded L-Leu-D-Phe-D-Phe anchored to each CNS as shown in Scheme 1. The products of each synthetic step were characterized by thermogravimetric analysis (TGA) (Table 1) and colorimetric Kaiser tests to assess the presence of primary amino groups (Figure S8). Raman spectroscopy (Figures S9–S10) and TEM micrographs (Figure S11) confirmed the preservation of CNS structures after their covalent functionalization.

Table 1. Thermogravimetric analysis (TGA) data for CNS functionalization steps. Average weight loss (%) at 600°C is reported (+−standard deviation) and the corresponding mmol/g are provided between brackets. *mmol are calculated considering solely the presence of COOH groups.

CNS	Oxidation	+ linker	+ peptide
CNHs	9.8 ± 0.6	10.8 ± 1.0	12.5 ± 0.9
	(2.2 ± 0.13)*	(0.62 ± 0.06)	(0.22 ± 0.02)
MWCNTs	9.2 ± 0.4	10.9 ± 1.3	12.0 ± 1.7
	(2.0 ± 0.08)*	(0.62 ± 0.07)	(0.21 ± 0.03)
G	10.2 ± 0.4	11.0 ± 0.5	n. a.
	(2.3 ± 0.08)*	(0.63 ± 0.03)	

Chemistry–A European Journal

Research Article
doi.org/10.1002/chem.202301708

Chemistry Europe
European Chemical
Societies Publishing

Successful covalent functionalization depends on CNS reactivity, which is higher for those with higher curvature, such as CNHs and CNTs. Indeed, oxidation conditions for the three CNSs were different to attain the same level of oxidation,[21] as calculated in terms of mmol of COOH functional groups per gram of CNS (Table 1). Only 28–31% of the theoretical COOH groups further reacted with the linker, which was anchored to the same extent onto the three CNSs (*i.e.*, 0.62–0.63 mmol/g as shown in Table 1). Similarly, 34–35% of the linker was successfully coupled to L-Leu-D-Phe-D-Phe (*i.e.*, 0.21–0.22 mmol/g, last column of Table 1), but only in the case of CNHs and CNTs. Indeed, both CNSs showed increasing amounts of weight loss along the functionalization steps (Table 1), and according changes in I_D/I_G intensities in the Raman spectra (Table S1). Qualitative ninhydrin tests confirmed the successful derivatization with color changes indicative of the presence of protected or unprotected primary amines, as expected after each step (Figure S8).

Conversely, GO was more difficult to functionalize. TGA data and ninhydrin tests confirmed successful attachment of the linker (Table 1 and Figure S8), while no significant differences were found after reaction with the peptide, despite numerous attempts with different reaction conditions. It is possible that the Fmoc-tripeptide preferably adsorbed onto the GO surface, and/or that GO promoted nucleation of peptide stacks that rendered it not easily accessible for further reactions.[23] Therefore, only the functionalized CNHs (fCNHs) and CNTs (fCNTs) were retained for further tests.

Nanoscale characterization of free peptide coating onto functionalized CNSs (fCNSs)

Nanocomposite hydrogels were obtained using an optimized procedure, by dispersing the functionalized CNSs and the self-assembling tripeptide in an alkaline phosphate solution.[21] Subsequent dilution with an equivalent volume of a mildly acidic phosphate buffer triggered peptide self-assembly at neutral pH. We employed analogous conditions as those previously tested with the highest loading of oxCNHs and oxCNTs (*i.e.*, 1 mg/ml). In this way, the effect of covalently anchoring the peptide onto the fCNSs on the self-assembly behavior of the tripeptide could be assessed and compared with previous data on oxCNSs.

First of all, TEM imaging was carried out on the precursor solutions prior to self-assembly to assess any improvement in the coating of the fCNSs enabled by the covalent attachment of the peptide onto their surface, relative to oxCNSs. fCNHs displayed a thick, although irregular, coating by the peptide (Figure 1A–B, and Figure S13), with reduced self-aggregation relative to analogous samples with oxCNHs.[21] The vast majority of fCNHs displayed partial coating of their surface, with a large exposed bare area of their graphitic surface (Figure S13). The thickness of the organic coating was highly variable, often reaching several tens of nanometers.
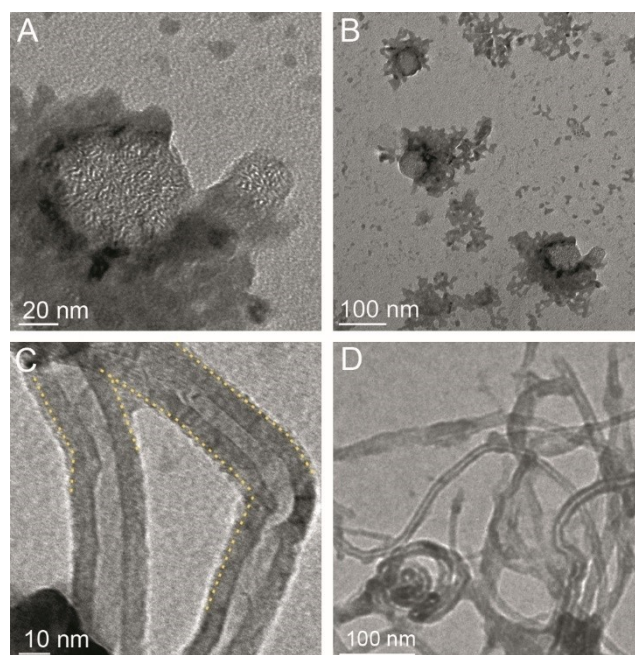

Figure 1. Transmission electron microscopy (TEM) images of peptide gel-precursor dispersions of functionalized CNHs (A–B) and MWCNTs (C–D) with anchored peptide at higher (A,C) and lower (B,D) magnification. Yellow dotted lines in C trace the contour of the graphitic walls of CNTs to guide the eye.

In the case of fCNTs, their surface coating was just a few nm-thin and incomplete (Figure 1C–D and Figure S14). The anchoring of the peptide thus did not favor a complete coating by the free peptide in solution onto the fCNTs, rather the opposite. Indeed, there were many instances of uncoated fCNTs (Figure S14), in contrast with the oxCNTs without anchored peptide, which displayed a uniform peptide coating throughout.[21] It is possible that the free peptide coating onto fCNSs was hindered also by the presence of unreacted linker, which could partially hinder the ability of the graphitic surface to establish hydrophobic interactions with the aromatic Phe rings.

Nanoscale characterization of supramolecular hydrogels with functionalized CNSs (fCNSs)

Next, the pH trigger was applied to obtain the self-organization of the zwitterionic peptide in solution into a hydrogel. TEM imaging of the nanocomposite with fCNHs revealed a dense network of peptide fibrils with fCNHs mostly anchored onto them (Figure 2A), in contrast with the nanocomposite hydrogel obtained with free tripeptide and oxCNHs, which displayed oxCNH aggregates not interacting with the peptide fibrils (Figure 2B), as previously found.[21] These data confirmed that the covalent anchoring of the tripeptide onto the fCNHs favored the interaction with the free peptide, as intended by design, and solved the issue of oxCNH segregation. The nanocomposite hydrogels with fCNTs revealed a highly interconnected network where it was difficult to distinguish
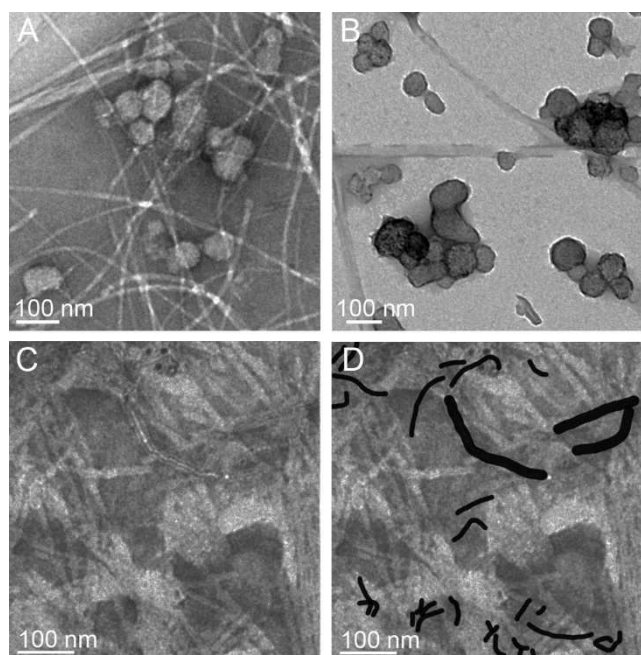
Chemistry–A European Journal

Research Article
doi.org/10.1002/chem.202301708

Chemistry Europe
European Chemical
Societies Publishing

Figure 2. TEM images of nanocomposite tripeptide gels with fCNHs (A), oxCNHs (B), or fCNTs (C–D). fCNHs with anchored peptide (A) do not show segregation form peptide fibrils observed in the case of oxCNHs[21] (B). fCNTs (C) are difficult to distinguish from peptide fibrils and are traced in black in (D) to guide the eye.

between peptide fibrils and fCNTs (Figure 2C), suggesting a high level of interaction between the two, similarly to the case of oxCNTs (Figure S12). We inferred that, in this case, the morphological similarity between the tubes and the fibrils played a more dominant role, relative to the CNT functionalization *per se*, to yield the interconnected network forming the gel matrix.

In the self-assembly process, first the peptide stacks into fibrils, which then can bundle into fibers. We thus analyzed more in detail the effect that each fCNS had on peptide fibrillation by measuring fibril and fiber diameters in the obtained nanocomposite hydrogels (Figure 3). In the case of fCNHs (Figure 3A), the average fibril diameter of 12.9 ± 2.9 nm (100 counts) was comparable to that of the hydrogel without CNHs or with oxCNHs (*i.e.*, 11.5 ± 2.2 nm and 10.9 ± 1.7 nm, respectively).[21] Conversely, the average fiber diameter was significantly reduced, as it corresponded to 21.1 ± 4.5 nm with fCNHs, relative to 44.2 ± 17.1 nm for the peptide-gel, and 34.5 ± 8.4 nm for the peptide-gel with oxCNHs. [21] We inferred that covalently anchoring of the peptide onto the fCNHs did not interfere with the free-peptide ability to fibrillate, rather with the fibrils' ability to bundle, probably as a result of the interactions between fibrils and peptide molecules bound onto fCNHs. This phenomenon was observed also when nitrogen-doped carbon dots were added to the peptide gel prior to, or during assembly, suggesting it is not unique of peptide-peptide interactions.[24]

In the case of CNTs (Figure 3B), TEM analysis of the nanocomposite gel revealed a broader distribution of fibril diameters, with a median value of 15.4 ± 5.7 nm. The significant

increase in fibrils' thickness was confirmed also at the level of fibers, whose average diameter corresponded to 29.8 ± 4.0 nm.

We can conclude that, upon covalent attachment of the self-assembling peptide onto fCNSs, fibrils' bundling was mainly occurring in pairs, and that the CNT morphology played a role in fibrillation, leading to thicker fibrils relative to the case of CNHs.

Macroscopic characterization of nanocomposite hydrogels with functionalized CNSs (fCNSs)

The hydrogels' viscoelastic properties were assessed by oscillatory rheometry. Our samples were true hydrogels, as confirmed by frequency sweeps (Figure S15), which were performed in the linear viscoelastic region (Figure S17), and which displayed both elastic and viscous moduli being independent from the applied frequency with $G' \gg G''$. Time sweeps (Figure S16) revealed immediate hydrogelation, confirming visual observations, with nanocomposite hydrogels reaching an elastic modulus of 3.48 ± 1.08 kPa in the case of fCNHs, and 4.27 ± 0.96 kPa in the case of fCNTs. Both hydrogels showed a modest increase in the elastic moduli relative to the peptide gel without fCNSs (*i.e.*, 2.0 ± 0.1 kPa).[21] We inferred that the expected increase in stiffness due to the addition of fCNSs was counterbalanced by the reduced peptide bundling in their presence, thus leading to networks of thinner fibers overall. Interestingly, using one tenth of each CNM (*i.e.*, 0.1 mg/ml) led to similar results (Figure S18–S20), thus indicating the presence of nonlinear effects. The only significant difference was the reduced
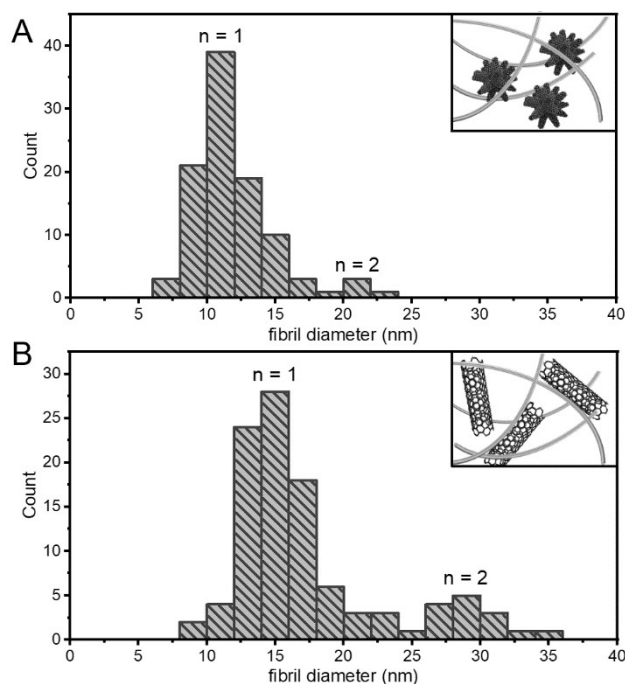

Figure 3. Peptide fibril diameter analysis from TEM micrographs of gel nanocomposites with fCNHs (A) or fCNTs (B). The majority were individual peptide fibrils (n = 1) with some instances of fibril pairs (n = 2).

Chemistry–A European Journal

Research Article
doi.org/10.1002/chem.202301708

Chemistry
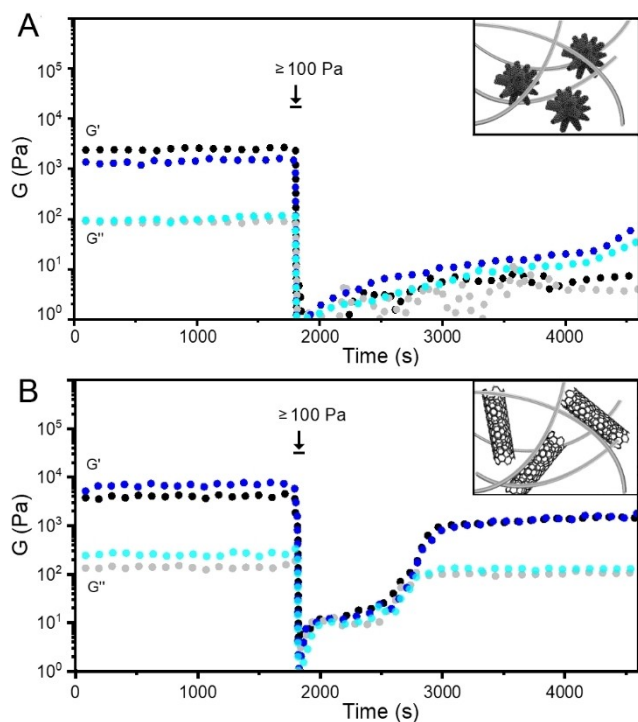Europe
European Chemical
Societies Publishing

Figure 4. Stress-recovery rheological tests for nanocomposites with fCNHs (A) or fCNTs (B) revealed self-healing ability only for the latter upon gel breaking with a 30 s-pulse at ≥ 100 Pa (arrow). Two independent replicas are shown.
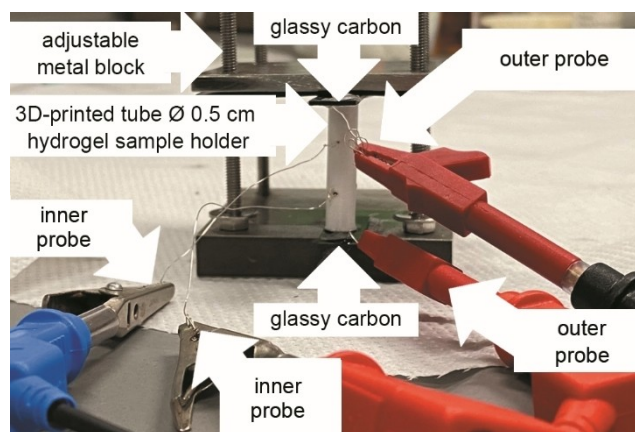

Figure 5. Experimental setup for the conductivity measurements.

Figure 5. Control experiments performed on peptide gels without fCNSs, and with doubling concentrations of phosphate buffer, demonstrated that the mobile ions were mainly responsible for the observed conductivity, which roughly doubled with each 2-fold increase in sodium phosphate concentration. In the presence of phosphate buffer, any increase in conductivity due to the presence of fCNSs was negligible. As the phosphate buffer concentration increased 2-fold and 4-fold, from 50 mM, to 100 mM and to 200 mM, the conductivity increased from 2.8, to 4.7, to 13.2 mS/cm (Table 2). The tested nanocomposites with fCNSs displayed a conductivity of 4.9–5.0 mS/cm (Table 2). For reference, these values are within range of those found for human conductive tissues, such as the brain grey matter (4.2 ± 2.3 mS/cm for grey matter), the cerebellum (5.8 ± 1.9 mS/cm), the heart (6.6 ± 1.1 mS/cm for the heart lumen, 3.9 ± 1.5 mS/cm for the heart muscle), muscles (4.6 ± 2.4 mS/cm), nerves (3.5 ± 1.9 mS/cm) and spinal cord (6.1 ± 1.3 mS/cm).[25]

Conclusions

In conclusion, this work revealed that anchoring of the self-assembling peptide onto fCNHs was a successful strategy to promote their coating by the free peptide in solution, to avoid their segregation from the peptide in the nanocomposite hydrogels. Interestingly, addition of fCNTs provided the nanocomposite with self-healing ability, which was absent in the case of the peptide gel without CNTs or the one with fCNHs. This work demonstrated that the self-healing ability is thus not due to the interaction between free peptide gelator and anchored peptide onto the fCNSs, rather it can be ascribed to the interaction between anisotropic CNTs and peptide fibrils.

Overall, this work deepened our understanding of these materials at the interface between nanotechnology and supramolecular chemistry and confirmed an elected role played by CNTs to yield highly interconnected matrices with peptide fibrils that acquire self-healing ability. Given the importance of anisotropic nanostructures in a variety of applications, such as guiding neurons' growth direction,[26] future applications are envisaged in neuroscience. Furthermore, the inclusion of bioactive peptide motifs[27]

linear viscoelastic region for the nanocomposites with CNHs (Figure S20), relative to those with higher loadings (Figure S17).

Interestingly, stress-recovery tests (Figure 4) showed that, upon breaking of the gel matrix with a 30 s-pulse at ≥ 100 Pa, the reformed gels were only those with fCNTs (both at 1 mg/ml or 0.1 mg/ml, Figure S21)– and not those with fCNHs (at both loading levels, Figure 4 and Figure S21)– although the recovery of the original viscoelastic properties was not in full. These findings confirmed that it is the anisotropic morphology of CNTs that enables the self-healing ability, and not the quality or quantity of peptide coating onto their surface. Furthermore, no significant increase in the gel resistance against applied stress was found upon inclusion of either fCNS (Figure S15), suggesting that the covalent anchoring of the peptide onto the fCNSs did not, in fact, improve the interconnectivity between peptide fibrils upon intercalation of fCNSs.

Finally, we performed conductivity measurements (Table 2) using the four-probe method and the experimental setup shown in

Table 2. Conductivity measurements (mS/cm) on the peptide hydrogels without or with CNSs, and controls with peptide hydrogels.

Hydrogel	50 mM[a]	100 mM[a]	200 mM[a]
Peptide	2.8 ± 1.3	4.7 ± 1.8	13.2 ± 5.9
CNHs	–	4.9 ± 0.59	–
MWCNTs	–	5.0 ± 0.15	–
[a] phosphate buffer concentration.			

Chemistry–A European Journal

Research Article
doi.org/10.1002/chem.202301708

Chemistry Europe
European Chemical
Societies Publishing

could be explored as a strategy to provide selectivity in sensing, where CNTs have great potential in terms of applicability.[28] Bioinspired and biomimetic actuation is another area that bears scope for further development,[29] and that may benefit from these studies.

Experimental Section

Materials and general methods

CNHs were supplied by Carbonium s.r.l. (Italy). Elicarb multi-walled CNTs (ref. PR0940, batch 71967/35, purity 70–90%) and Elicarb premium-grade graphene (G) powder (ref SP8073P, batch L4002B, 6.6 layers average thickness, >4% organic residue and >4% oxide residue) were kindly provided by Thomas Swan and Co. Ltd. (UK). Solvents and chemicals were obtained from Merck (Italy) and they were used as received. High-purity Milli-Q water with a minimum resistivity of 18.2 MΩ·cm@25 °C was dispensed from a Milli-Q Academic System (Millipore RiOs/Origin purification system, St. Louis, MS, USA) and used to prepare all solutions and buffers. CNS dispersions were sonicated for 15 min. in a Branson Ultrasonic 3800 cleaning bath (Milan, Italy) as indicated in the functionalization protocol below. All CNS filtrations during washes were performed in a Millipore pyrex apparatus with a Millipore membrane filter (JHWP, 0.45 μm). TGA, TEM, Raman spectroscopy, and oscillatory rheometry were carried out as previously described.[22]

CNS functionalization

CNHs, CNTs, and G were oxidized as previously described.[21] Attachment of the linker N-Boc-2,2′-(ethylenedioxy)diethylamine (2.5 eq. based on the estimation of 2.5 mmol/g of COOH on each CNS) was performed in a solution of 1 mL MES buffer (0.1 M, pH 6.0) that was added to a dispersion of CNSs (20 mg) with sulfo-NHS (2.5 eq) and EDC-HCl (2.5 eq) in 20 mL of MES buffer pH 6 that was previously stirred and sonicated in a 100-mL round-bottom flask. The mixture was stirred for 24 h at room temperature. The black powder was washed five times with deionized water, thrice with methanol, twice with deionized water, twice with methanol, and finally with diethyl ether to dry in vacuo. Boc-deprotection was performed by stirring overnight a dispersion of each CNS in a solution of HCl 6 M (20 mL) in methanol (20 mL) that was previously sonicated for 20 min. to disperse the CNSs. Washes were performed thrice with water, thrice with methanol, and once with diethyl ether. Peptide coupling was performed by dissolving Fmoc-L-Leu-D-Phe-D-Phe[22] (3 eq.), HBTU (2.5 eq.) and HOAt (2.5 eq.) 5 mL of DMF, and then adding 100 μL of DIPEA 1 M, resulting into a pale-yellow solution, which was added dropwise to a dispersion each CNS (15 mg) in 15 mL DMF that was previously sonicated at room temperature for 15 min. The reaction was allowed to proceed for 24 h. The black powder was washed four times with DMF, thrice with deionized water, once with methanol, and then once with diethyl ether to then be dried in vacuo. Fmoc-deprotection was performed for 30 min. by dispersing each CNS (0.5 mg/mL) in piperidine (20%) in DMF, through sonication. The black powder was washed as in the previous step and dried in vacuo.

Nanocomposite hydrogel formation

Nanocomposite hydrogels were obtained using a pH trigger. Firstly, L-Leu-D-Phe-D-Phe[21] (5 mg) was dissolved in an alkaline sodium phosphate solution (1 mL, 0.1 M, pH 11.8) with the aid of sonication for 5 minutes. Next, 1 mL of mildly acidic sodium phosphate buffer (0.1 M, pH 5.8) was added to reach pH neutrality and yield the peptide

hydrogel that was used as a control. In the case of nanocomposites, the same protocol was modified by including 2 mg of peptide-functionalized fCNS in the alkaline sodium phosphate buffer, and sonicating for 15 min. to obtain homogeneous dispersions.

Stress-recovery experiment

Each gel was freshly prepared onto the plate of a stress-controlled rotational rheometer Haake MARS III equipped with a Peltier temperature control system. 20 mm titanium grooved plates were used for all measurements with a gap of 0.700 mm. The alkaline sample with peptide and fCNSs was placed onto the plate, and the second buffer was placed atop to induce the pH-triggered gelation. The standard solvent trap provided with the rheometer was gently placed around the sample and the measurements started. First, a time sweep was recorded for 30 min. at 2 Pa and 1 Hz, followed by a stress impulse of 100 Pa (or 200 Pa, leading to the same results) for 30 s, and then another time sweep at 2 Pa and 1 Hz as shown in Figure 4. Each experiment was performed at least three times independently.

Conductivity measurements

Conductivity measurements were performed in the setup shown in Figure 5, which used a plastic cylinder with internal diameter of 0.5 cm and length of 3.0 cm (length of 1.17 cm between the inner Ag wire contacts, silver wires 0.25 mm diameter, 99.9% Aldrich) that was produced with an extrusion 3D printer (PRUSAi3 MK2). The cylinder was filled with freshly prepared hydrogels (589 μl) that were formed with one-by-one addition of the alkaline and acidic buffers (49 μl). Next, the sample holder was immediately sandwiched between two glassy carbon electrodes as shown in Figure 5, and conductivity measurements were performed by applying a ±1 V voltages. Each experiment was performed three times independently and average values ± standard deviation are shown in Table 2.

Supporting Information

The supporting information file includes TGA data, photographs of Kaiser tests, Raman spectra, TEM micrographs and their analysis, rheological data.

Conflict of Interests

The authors declare no conflict of interest.

Data Availability Statement

The data that support the findings of this study are available in the supplementary material of this article.

[1] V. Georgakilas, J. A. Perman, J. Tucek, R. Zboril, *Chem. Rev.* **2015**, *115*, 4744–4822.

[2] N. Martín, *Chem* **2019**, *5*, 733–738.

[3] J. Bartelmess, S. Giordani, *Beilstein J. Nanotechnol.* **2014**, *5*, 1980–1998.

[4] R. Rao, C. L. Pint, A. E. Islam, R. S. Weatherup, S. Hofmann, E. R. Meshot, F. Wu, C. Zhou, N. Dee, P. B. Amama, J. Carpena-Nuñez, W. Shi, D. L. Plata, E. S. Penev, B. I. Yakobson, P. B. Balbuena, C. Bichara, D. N. Futaba, S. Noda, H. Shin, K. S. Kim, B. Simard, F. Mirri, M. Pasquali, F. Fornasiero, E. I. Kauppinen, M. Arnold, B. A. Cola, P. Nikolaev, S. Arepalli, H.-M. Cheng, D. N. Zakharov, E. A. Stach, J. Zhang, F. Wei, M. Terrones, D. B. Geohegan, B. Maruyama, S. Maruyama, Y. Li, W. W. Adams, A. J. Hart, *ACS Nano* **2018**, *12*, 11756–11784.

[5] V. Georgakilas, J. N. Tiwari, K. C. Kemp, J. A. Perman, A. B. Bourlinos, K. S. Kim, R. Zboril, *Chem. Rev.* **2016**, *116*, 5464–5519.

[6] C. Rosso, G. Filippini, M. Prato, *ACS Catal.* **2020**, *10*, 8090–8105.

[7] N. Karousis, I. Suarez-Martinez, C. P. Ewels, N. Tagmatarchis, *Chem. Rev.* **2016**, *116*, 4850–4883.

[8] a) G. Bottari, M. Á. Herranz, L. Wibmer, M. Volland, L. Rodríguez-Pérez, D. M. Guldi, A. Hirsch, N. Martín, F. D'Souza, T. Torres, *Chem. Soc. Rev.* **2017**, *46*, 4464–4500; b) B. Dinesh, A. Bianco, C. Ménard-Moyon, *Nanoscale* **2016**, *8*, 18596–18611; c) S. Marchesan, M. Melchionna, M. Prato, *Fullerenes, Nanotub. Carbon Nanostruct.* **2014**, *22*, 190–195.

[9] a) M. Tonellato, M. Piccione, M. Gasparotto, P. Bellet, L. Tibaudo, N. Vicentini, E. Bergantino, E. Menna, L. Vitiello, R. Di Liddo, F. Filippini, *Nanomaterials* **2020**, *10*, 415; b) S. Eissa, N. Alshehri, A. M. A. Rahman, M. Dasouki, K. M. Abu-Salah, M. Zourob, *Biosens. Bioelectron.* **2018**, *101*, 282–289.

[10] a) S. A. M. Tofail, E. P. Koumoulos, A. Bandyopadhyay, S. Bose, L. O'Donoghue, C. Charitidis, *Mater. Today* **2018**, *21*, 22–37; b) K. Tadyszak, J. K. Wychowaniec, J. Litowczenko, *Nanomaterials* **2018**, *8*, 944.

[11] a) L. Bao, X. Cui, M. Mortimer, X. Wang, J. Wu, C. Chen, *Nano Today* **2023**, *49*, 101784; b) S. Marchesan, S. Bosi, A. Alshatwi, M. Prato, *Nano Today* **2016**, *11*, 398–401.

[12] Y. Hui, Z. Yan, H. Yang, X. Xu, W.-E. Yuan, Y. Qian, *ACS Appl. Bio Mater.* **2022**, *5*, 4741–4759.

[13] S. G. Alamdari, A. Alibakhshi, M. de la Guardia, B. Baradaran, R. Mohammadzadeh, M. Amini, P. Kesharwani, A. Mokhtarzadeh, F. Oroojalian, A. Sahebkar, *Adv. Healthcare Mater.* **2022**, *11*, e2200526.

[14] G. Speranza, *Nanomaterials* **2021**, *11*, 967.

[15] K. Gao, B. Wang, L. Tao, B. V. Cunning, Z. Zhang, S. Wang, R. S. Ruoff, L. Qu, *Adv. Mater.* **2019**, *31*, e1805121.

[16] a) L. Wang, Z. Liu, J. Zhang, *Nanoscale* **2022**, *14*, 13473–13489; b) M. Zhang, X. Xuan, X. Yi, J. Sun, M. Wang, Y. Nie, J. Zhang, X. Sun, *Nanomaterials* **2022**, *12*, 2721; c) M. Melchionna, P. Fornasiero, *ChemCatChem* **2017**, *9*, 3274–3284.

[17] a) E. Anaya-Plaza, A. Shaukat, I. Lehtonen, M. A. Kostiainen, *Adv. Healthcare Mater.* **2021**, *10*, 2001162; b) Y. Qian, S. Di, L. Wang, Z. Li, *J. Mater. Chem. B* **2021**, *9*, 6521–6535; c) L. Tanzi, M. Terreni, Y. Zhang, *Eur. J. Med. Chem.* **2022**, *230*, 114104; d) G. Cellot, L. Jacquemin, G. Reina, A. Franceschi Biagioni, M. Fontanini, O. Chaloin, Y. Nishina, A. Bianco, L. Ballerini, *ACS Appl. Nano Mater.* **2022**, *5*, 17640–17651.

[18] a) V. Wulf, E. Bichachi, A. Hendler-Neumark, T. Massarano, A. B. Leshem, A. Lampel, G. Bisker, *Adv. Funct. Mater.* **2022**, *32*, 2209688; b) S. Adorinni, P. Rozhin, S. Marchesan, *Biomedicine* **2021**, *9*, 570; c) J. K. Wychowaniec, M. Iliut, M. Zhou, J. Moffat, M. A. Elsawy, W. A. Pinheiro, J. A. Hoyland, A. F. Miller, A. Vijayaraghavan, A. Saiani, *Biomacromolecules* **2018**, *19*, 2731–2741.

[19] a) M. Reches, E. Gazit, *Science* **2003**, *300*, 625–627; b) L. Adler-Abramovich, L. Vaks, O. Carny, D. Trudler, A. Magno, A. Caflisch, D. Frenkel, E. Gazit, *Nat. Chem. Biol.* **2012**, *8*, 701–706.

[20] a) S. Alshehri, H. H. Susapto, C. A. E. Hauser, *Biomacromolecules* **2021**, *22*, 2094–2106; b) J. K. Sahoo, C. Nazareth, M. A. Vanden Berg, M. J. Webber, *Soft Matter* **2018**, *14*, 9168–9174; c) P. W. J. M. Frederix, G. G. Scott, Y. M. Abul-Haija, D. Kalafatovic, C. G. Pappas, N. Javid, N. T. Hunt, R. V. Ulijn, T. Tuttle, *Nat. Chem.* **2015**, *7*, 30–37.

[21] D. Iglesias, M. Melle-Franco, M. Kurbasic, M. Melchionna, M. Abrami, M. Grassi, M. Prato, S. Marchesan, *ACS Nano* **2018**, *12*, 5530–5538.

[22] D. Marin, M. Bartkowski, S. Kralj, B. Rosetti, P. D'Andrea, S. Adorinni, S. Marchesan, S. Giordani, *Nanomaterials* **2023**, *13*, 172.

[23] a) E. D. Sitsanidis, L. A. L. Dutra, J. Schirmer, R. Chevigny, M. Lahtinen, A. Johansson, C. C. Piras, D. K. Smith, M. Tiirola, M. Pettersson, M. Nissinen, *ACS Omega* **2023**, *8*, 10225–10234; b) R. Orbach, L. Adler-Abramovich, S. Zigerson, I. Mironi-Harpaz, D. Seliktar, E. Gazit, *Biomacromolecules* **2009**, *10*, 2646–2651.

[24] M. C. Cringoli, S. Kralj, M. Kurbasic, M. Urban, S. Marchesan, *Beilstein J. Nanotechnol.* **2017**, *8*, 1553–1562.

[25] C. Gabriel, *Compilation of the Dielectric Properties of Body Tissues at RF and Microwave Frequencies, Report N.AL/OE-TR-1996–0037, Occupational and environmental health directorate, Radiofrequency Radiation Division, Brooks Air Force Base*, Texas (USA), **1996**.

[26] S. Marchesan, L. Ballerini, M. Prato, *Science* **2017**, *356*, 1010–1011.

[27] a) C. Ligorio, A. Mata, *Nat. Rev. Bioeng.* **2023**, *1*, 518–536; b) I. W. Hamley, *Chem. Rev.* **2017**, *117*, 14015–14041.

[28] V. Schroeder, S. Savagatrup, M. He, S. Lin, T. M. Swager, *Chem. Rev.* **2019**, *119*, 599–663.

[29] L. Lu, W. Chen, *Nanoscale* **2011**, *3*, 2412–2420.